# Nanoscale

Accepted Manuscript


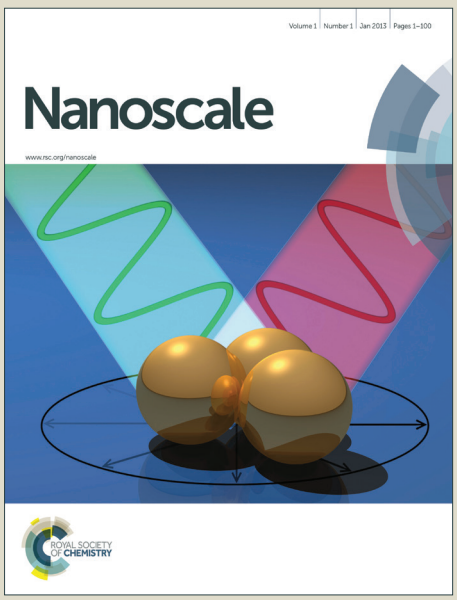





ROYAL SOCIETY OF CHEMISTRY

www.rsc.org/nanoscale

Journal Name

RSCPublishing

ARTICLE

# Controlled Surface Functionality of Magnetic Nanoparticles by Layer-by-Layer Assembled Nano-Films†

Cite this: DOI: 10.1039/x0xx00000x

Received 00th January 2012,
Accepted 00th January 2012

DOI: 10.1039/x0xx00000x

www.rsc.org/

Daheui Choi [a], Boram Son [b], Tai Hyun Park [*bc] and Jinkee Hong [*a]

Over the past several years, the preparation of functionalized nanoparticles has been aggressively pursued in order to develop desired structures, compositions, and structural order. Among the various nanoparticles, iron oxide magnetic nanoparticles (MNPs) show great promise because the material generated using these MNPs can be used in a variety of biomedical applications and possible bioactive functionalities. In this study, we report the development of various functionalized MNPs (F-MNPs) generated using the layer-by-layer (LbL) self-assembly method. To provide broad functional opportunities, we fabricated F-MNPs bio-toolbox by using three different materials: synthetic polymers, natural polymers, and carbon materials. Each of these F-MNPs displays distinct properties, such as enhanced thickness or unique morphologies. In an effort to explore their biomedical applications, we generated basic fibroblast growth factor (bFGF)-loaded F-MNPs. The bFGF-loaded F-MNPs exhibited different release mechanisms and loading amounts, depending on the film material and composition order. Moreover, bFGF-loaded F-MNPs displayed higher biocompatibility and possessed superior proliferation properties than the bare MNPs and pure bFGF, respectively. We conclude that by simply optimizing the building materials and the nanoparticle film composition, MNPs exhibiting various bioactive properties can be generated.

## Introduction

In recent years, nanoparticles have been consistently used for various biomedical applications, including drug delivery, gene delivery, tissue engineering, and biomedical imaging[1-4]. Nanoparticles can be used in various biomedical applications because they exhibit a high degree of stability and loading capacity and can be efficiently modified to achieve the desired functionalities [5-8]. Moreover, nanoparticles possess unique physical and chemical properties, which are not shown by bigger particles, due to a high surface-to-volume ratio[9,10]. In order to use nanoparticles for designing biomedical applications, we need elaborate technologies that can precisely control the required chemical functionality[11]. So far, the functionalization of nanoparticles has been mainly focused on the chemical conjugation of nanoparticles and bioactive materials to other bulk materials[12-16]. Such a conjugation method allows high stability under physiological conditions, enhanced cellular uptake, and selectivity, and is therefore widely utilized for in vivo imaging probes, diagnostics, and therapeutics[14,17-19]. However, there are some difficulties with the conjugation method on precisely controlling modified thickness, morphologies, deposition, layer degradation, and incorporation onto nanoparticles with multiple kinds of biomaterials at once[20]. A more effective method for nanoparticle functionalization is needed.

The layer-by-layer (LbL) self-assembly method is a multilayer nanofilm buildup process at the molecular level, involving the repetitive adsorption of oppositely charged polymers[21-24]. The LbL assembly method is known to be simple, versatile, and inexpensive and can be used to prepare nanosized-controlled multilayer films with varying composition and structure[22,25-28]. Unlike other well-known nano-sized film fabrication methods involving self-assembly monolayers (SAMs) and Langmuir-Blodgett films, LbL assembly can be incorporated into water-soluble materials, including biocompatible polymers, DNA, and proteins, up to the desired deposited order, thickness, roughness, and so on[29,30]. Moreover, the LbL films can create nanoscale blended features within each material that cannot be simply realized by the traditional mixing method[31]. In order to take advantage of the LbL self-assembly method, recently, nanoparticles functionalized with LbL films have been extensively developed for various biomedical applications after Gittins and Caruso first reported LbL nanofilms on gold nanoparticles with polyelectrolytes[2,22,32,33]. Poon et al. (2011) fabricated hyaluronic acid- and dextran sulfate-incorporated nanofilms onto quantum dots and gold nanoparticles and demonstrated an increased biostability and biodistribution capacity of the generated particles[34]. Schneider et al. (2009) generated LbL-assembled multilayer films on gold nanoparticles and investigated their anti-cancer and stealth properties[35]. However, many reports have been focused on polyelectrolytes as building materials for LbL films on nanoparticles[34,36-38]. In order to assign additional bio-

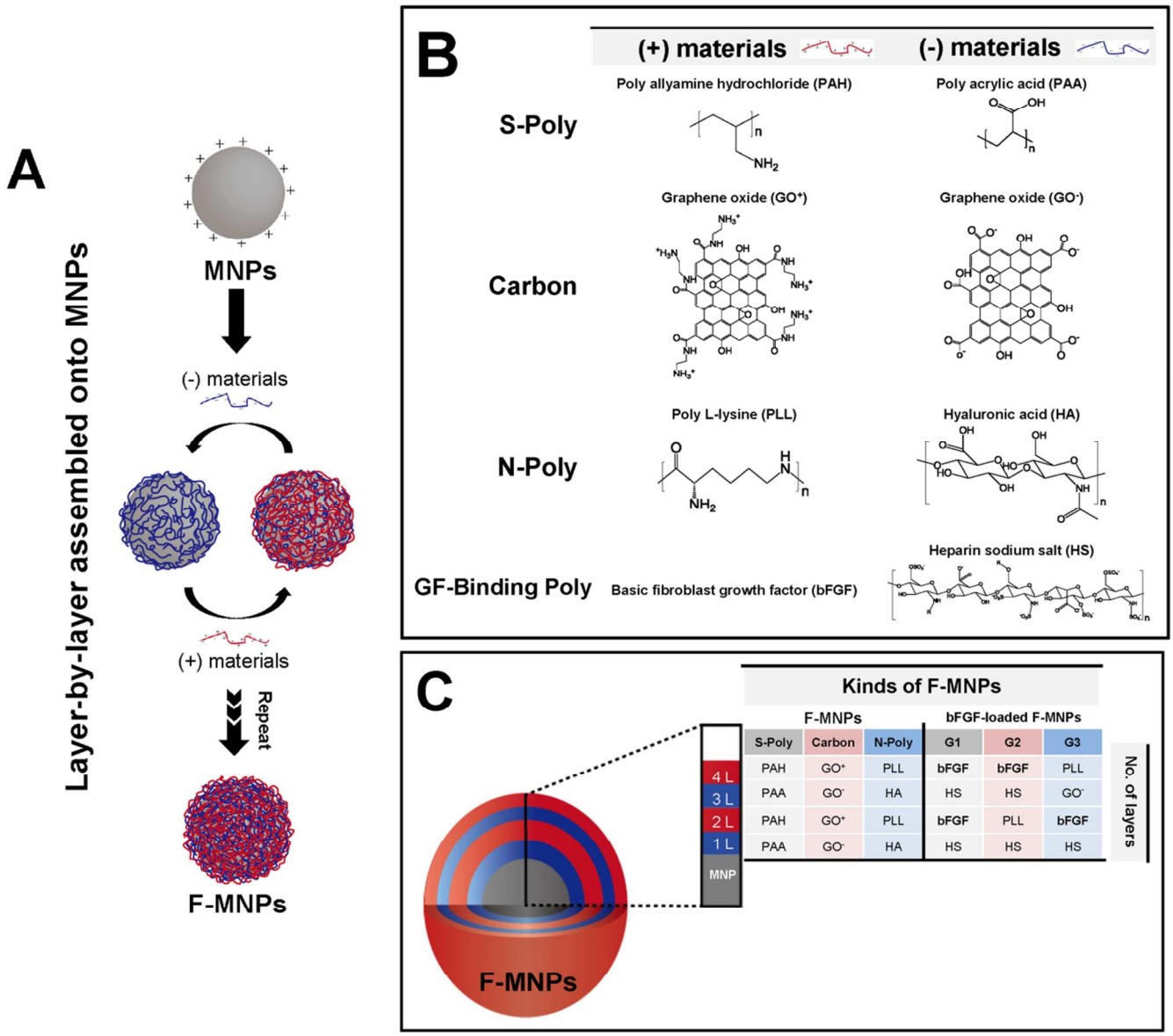


**Figure 1.** (A) Schematic illustration of LbL deposition process onto MNPs. (B) The structures of LbL components used in this paper. Positively and negatively charged materials are displayed in the left and right columns, respectively. Each row is grouped by material properties such as S-Poly, Carbon, N-Poly and GF(growth factor)-Binding Poly. (C) Schematic illustration of various kinds of F-MNPs. The left image illustrates the internal structure of F-MNPs. The table on the right lists the types of F-MNPs used in this study. The F-MNPs have been divided into two categories, viz. various materials-loaded (VMs-loaded) and bFGF-loaded F-MNPs. Each section comprises S-poly (synthetic polymers), carbon (carbon materials), and N-poly (natural polymers) for the F-MNPs, and G1 (growth factor), G2, and G3 for the bFGF-loaded F-MNPs, respectively

functional properties, more candidate materials that can be incorporated into LbL films are needed.

In this study, we have prepared and characterized various LbL multilayer film structures on iron oxide magnetic nanoparticles (MNPs), and have investigated their cell viability and proliferation. In particular, we first demonstrated protein- or graphene oxide (GO)-incorporated functionalized-MNPs (F-MNPs) to assign direct cell proliferation or additional barrier effects. We preferred using the LbL self-assembly method to design the various kinds of F-MNPs. By using this method, we could easily control the F-MNPs' internal film structure, morphology, and protein loading and release rate. With bFGF-incorporated F-MNPs, the bFGF release kinetics could be controlled from burst release profile within 2-3 days to sustained release profile for 10 days. Also the films reduce toxicity of MNPs and enhance fibroblast proliferation compared with bare bFGF. The procedures used for preparing F-MNPs have been described in Figure 1A. The MNPs possess a positive surface charge; therefore, the negatively charged polymers can be easily applied onto the MNPs without any additional functionalization. Each layer can be continuously stacked by the alternative adsorption of oppositely charged materials, resulting from the over-compensation of the surface charge during the deposition process[21,39,40]. We have built up

four layers of F-MNPs by using different materials, such as synthetic and natural polymers (S-Poly & N-Poly), carbon materials, and protein to realize the possibilities of nanoparticle functionalization without limitation on the use of materials; a strong advantage of the LbL self-assembly method. Poly(acrylic acid) (PAA) and poly(allylamine hydrochloride) (PAH) are the synthetic weak polyelectrolytes that are typically used as ingredients for the LbL films[41]. The two-dimensional carbon nanomaterial derived from GO possesses its own unique physical, chemical, and electrical properties, and is therefore a promising material that can be used for various applications[42,43]. Owing to its enhanced physical and chemical strength for drug release, GO was also used as multilayer components for F-MNPs. The positively and negatively charged GOs also show a weak polyelectrolyte behavior for the treatment of chemical oxidation and modification of functional groups, i.e., carboxylic acid and amine groups. Lastly, we chose two representative natural polymers, poly-L-lysine (PLL) and hyaluronic acid (HA), as film components. The polypeptide PLL and polysaccharide HA have been widely used as LbL components for biomedical approaches, such as drug delivery systems or tissue engineering, over several decades[36,44-46]. During this study, we prepared three different types of composite films (S-Poly, Carbon, and N-Poly) and characterized their morphologies, thicknesses, and surface charges. Additionally, we also used basic fibroblast growth factor (bFGF)-loaded F-MNPs to control cell culture activity by growth factor delivery from MNPs. The bFGF is known to be the primary growth factor responsible for generating new vascular endothelial cells and also contains essential ingredients for cell proliferation and differentiation of stem cells[47-49], and is mainly used for wound healing during brain and skin injury[50,51], as well as treating peripheral arterial diseases (PADs)[52,53]. In addition, bFGF harbors a heparin-binding domain, and therefore, binds with the heparin sodium salt (HS) with high affinity. This domain is an anionic sulfated glucosaminoglycan that plays a major role in blood anticoagulation by enhancing the stability and activity of bFGF[54-56]. Thus, bFGF and HS can bind strongly owing to structural affinity and favorable electrostatic interactions. For this reason, we prepared bFGF- and HS-incorporated F-MNPs in order to enhance the efficacy of the delivery process mediated by the protein carrier. Furthermore, we deposited various functional materials into the multilayers. PLL, a linear polypeptide, was assembled in such a way as to induce more bFGF into the multilayer. We also used the carbon material GO as a protein barrier with a low permeability (see Figure 1). Finally, we studied the in vitro proliferation of human dermal fibroblasts (hDFs) in order to examine the effectiveness of F-MNPs as protein carriers.

## Experimental

### Materials

Iron (II) chloride tetrahydrate, dodecylamine, poly(acrylic acid) (PAA, $M_w$ 2,000), poly(allylamine hydrochloride) (PAH, $M_w \approx$ 15,000), poly-L-lysine solution (PLL, $M_w$ 70,000–150,000, 0.01% in $H_2O$), hyaluronic acid sodium salt (HA, from *Streptococcus equi*), and heparin sodium salt (HS, from porcine intestinal mucosa) were purchased from Sigma-Aldrich. Basic fibroblast growth factor (bFGF, recombinant human protein), α-minimum essential medium (α-MEM, no nucleosides), fetal bovine serum (FBS), penicillin-streptomycin (PS), and trypsin-EDTA (TE) were obtained from Gibco® Life Technologies. Dulbecco modified eagle medium (DMEM) was purchased from Thermo Scientific. Float-A-lyzer® G2 (MWCO, 50 kDa) was purchased from the Spectrum Lab. Phosphate buffered saline (PBS) was purchased from Biosolutions, Inc. Human dermal fibroblasts (hDFs) were purchased at passage 1 from ATCC. Positively and negatively charged GO was synthesized by Hummers method according to a previous paper[57]. The GO size and structure were confirmed by atomic force spectroscopy (AFM, Park Systems X-10) and is shown in Figure S3†.

### Synthesis of MNPs

The MNPs were synthesized following a one-step process for the amine-stabilized MNPs, previously reported by Aslam et al[58]. Briefly, a 40 mM dodecylamine solution in 100 mL of $H_2O$ was stirred and heated to 85 °C. Subsequently, 10 mM of ferrite chloride ($FeCl_2 \cdot 4H_2O$) was added to the dodecylamine solution, at which time the solution immediately turned black and yielded MNPs. The mixture was vigorously stirred for about 3 h at 85 °C and centrifuged thereafter to obtain the MNPs. The MNPs were dispersed in $H_2O$ and stored at ambient temperature.

### Fabrication procedure for the F-MNPs

The F-MNPs (for S-Poly, Carbon and N-Poly) were prepared with the centrifugation layer-by-layer assembly method. The fabrication procedures for the F-MNPs were as follows: First, 30 μL of the MNPs solution was diluted with 0.5 mL of $H_2O$. The MNPs solution was then purified by dispersion and centrifugation for 10 min at 12,000 rpm. Subsequently, the supernatant $H_2O$ was removed, and 0.6 mL of the first negatively charged layer polymer solution was added. The mixture was dispersed by sonication and vigorous vortexing for 5 min. Following the 5 min deposition process, the suspension was centrifuged for 5 min at 12,000 rpm. The remaining unbound polymer was removed with two additional wash steps by adjusting the pH. Then, 0.5 mL of deionized (DI) $H_2O$ was added and the material was centrifuged for 5 min at 12,000 rpm. The process was repeated four times to fabricate four layers on the F-MNPs. The deposition pH conditions were 6.5 and 3.5 for S-Poly, 3.5 for Carbon, and 6.0 for N-Poly. The polymer solution concentration was 0.5 mg/mL in $H_2O$, whereas that for the PLL and GO solution was 5 μg/mL and 0.0125 wt%, respectively. The bFGF-loaded F-MNPs were prepared similarly by the method described above. All of the film ingredients were dispersed in 1X PBS buffer (pH 7.4) to achieve a final concentration of 0.5 mg/mL for all the solutions, except for the bFGF solution, for which it was 0.125 μg/mL. GO was dispersed in $H_2O$ at 0.0125 wt% adjusted pH at 3.5. The method used for preparing the F-MNPs is illustrated in Figure 1A.

### Film preparation

The bFGF-loaded multilayer films were fabricated onto a silicon wafer or quartz glass substrate and pre-treated for 10 min with RCA to clean and functionalize the negatively charged surface followed by previous paper[27]. Each layer was constructed by dipping the substrate into bFGF, PLL, HS, and GO solutions for 10 min and by subsequently washing it thrice with non pH-adjusted $H_2O$ for 2, 1, and 1 min. The dipping solutions were prepared in 100 mM NaOAc buffer (sodium acetate buffer; SAB) and the concentration of each component was 1 mg/mL for HS, 10 μg/mL and 0.1 μg/mL for bFGF. GO was dispersed in $H_2O$ at 0.05 wt%.

### Characterization of F-MNPs and multilayer films

Energy Filtering-Transmission Electron Microscopy (EF-TEM) images were obtained using a LIBER 120 microscope (Carl Zeiss), and the ζ-potential results were obtained using an SZ-100 Horiba

nanoparticle analyzer. The thicknesses of multilayer films on wafers were measured by profilometer (Dektak 150, Veeco). HS absorbance was confirmed by UV-visible spectrometer (V-670, Jasco).

### Release Characterization

The bFGF-loaded F-MNPs were dipped into 15 mL of α-MEM. More specifically, the 10mg of F-MNPs were mixed with 1 mL of α-MEM and dropped into Float-A-lyzer dialysis. After adding into the membrane, the membrane was placed into 50 mL conical tube then added 15 mL of α-MEM. The molecular weight cut off (MWCO) of the membrane was approximately 50 kDa. Therefore the bFGF is spontaneously released out to membrane. Then we collected 0.3 mL of α-MEM at various time points and added same quantity of fresh α-MEM into the conical tube. The released bFGF was measured using an enzyme-linked immunosorbent assay.

### Cell preparation

To examine cytotoxicity of magnetic nanoparticles, a Cell Counting Kit-8 (WST-8) assay was done. The WST-8 assay is based on the conversion of the tetrazolium salt, WST-8, to highly water-soluble formazan by dehydrogenase in living cells. The amount of yellow-color formazan dye generated by the reaction is measured to detect the number of viable cells. After the incubation of cells with magnetic nanoparticles of various concentrations in 96-well plates for 24 h at 37 °C in a humidified $CO_2$ incubator, cells were incubated with cell culture medium supplemented with 10% WST-8 solution for an additional 2 h in the incubator. The absorbance of each well was then measured at 450 nm.

### Cell proliferation test

The hDFs were seeded in 6-well plates. The cells were incubated with magnetic nanoparticles by loading 10 pg/mL of the bFGF in each well, for 0 to 14 days without medium replacement. The cell proliferation was determined by counting the number of cells with a hematocytometer after detaching the cells from the plates by using 0.25% TE.

## Results and discussion

### Analysis of F-MNPs

Figure 1B and 1C illustrate the various kinds of F-MNPs prepared during this study. The F-MNPs comprise an MNP with LbL multilayers deposited on its surface through electrostatic interactions and partial hydrogen bonding. The carbon F-MNPs bind with π–π interaction as well as electrostatic interaction[59]. For bFGF and HS (bFGF-loaded F-MNPs), additional structural binding occurs as well as electrostatic interaction and hydrogen bonding. The MNPs possess a positively charged surface owing to dodecylamine, as indicated by a ζ-potential of approximately 24.2 ± 3.4 mV (Figure S1†), which makes it feasible to assemble the multilayer film. The MNP cores are monodisperse and show spherical structures in the size range 20–30 nm, according to the TEM results. We displayed TEM images of MNPs and summarized size distribution and ζ-potential results in Figure S1†. As shown in Figure 1B, each column and row depict the various kinds of F-MNPs and the number of layers, respectively. We deposited six different film combinations of F-MNPs, abbreviated (in the accompanying text) according to their specific properties. The F-MNPs, the synthetic polymers PAA/PAH-loaded carbon material $GO^-/GO^+$ multilayer films, and natural polymer HA/PLL-loaded F-MNPs are simply designated as S-poly,

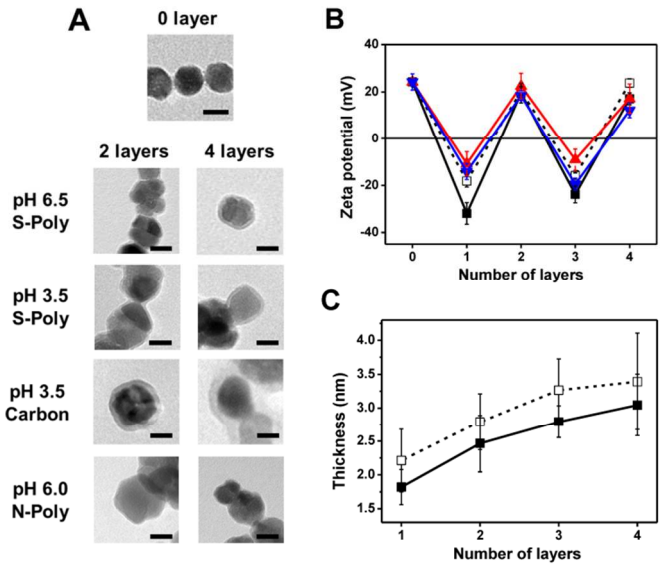


**Figure 2.** (A) EF-TEM micrographs of the MNPs and F-MNPs. The upper image displays the bare MNPs (0 layers), the images in the left column show the two layers deposited onto the MNPs, and the right column images show the four layers F-MNPs at various compositions (scale bar: 20 nm). (B) The zeta-potential measurements on the F-MNPs as a function of the number of layers: pH 6.5, S-poly (■, black line); pH 3.5, S-Poly (□, black dashed line); pH 3.5, Carbon (▲, red line); and pH 6.0, N-Poly (▼, blue line). The S-Poly thickness per layer, as a function of the pH conditions, is shown in (C): pH 6.5, S-poly (■, black line); pH 3.5, S-Poly (□, black dashed line). The original full-names of each of the F-MNPs are as follows: S-Poly, $(PAA/PAH)_2$; Carbon, $(GO^-/GO^+)_2$; and N-Poly, $(HA/PLL)_2$

Carbon, and N-poly, respectively. In order to assign various bFGF loading amounts and release kinetics to bFGF-loaded F-MNPs, we prepared 3 different bFGF-loaded films onto MNPs. The bFGF-loaded F-MNPs are labelled as G1, G2, and G3 (growth factor). G1 is only incorporated into the HS and bFGF composition, and PLL and $GO^-$ are additionally incorporated into G2 and G3, respectively.

The morphologies and ζ-potential results for each layer of the F-MNPs are indicated in Figure 2. As shown in Figure 2A, the multilayer thicknesses for S-poly and Carbon regularly increased as the number of layers increased. For the S-poly F-MNPs, we deposited multilayers at a pH of 3.5 and 6.5 to compare film thickness depending on pH conditions. PAH and PAA are weak polyelectrolytes whose degree of ionization varies significantly depending on the pH value. In other words, the polymers show loops, tails, and train chain conformations in different pH environments[41]. Moreover, during the LbL assembly, the film thickness and the morphology is highly affected by the previously adsorbed layer[41,60]. At a pH of 3.5, the degree of ionization of the PAA chain is >30% and that of PAH is >95%[61]. In contrast, the charge density of all the polymers at a pH of 6.5 is close to 100%. A relatively low charge density is observed at a pH of 3.5, and the polymers show higher portions of charged segments (as compared to the neutral segments). These charged segments comprise loops and tails, resulting in films that are thicker and rougher. The TEM images of the two layers for S-Poly at pH values 6.5 and 3.5 are depicted in Figure 2A. The thicknesses are approximately 2.5 nm and 2.73 nm, respectively. In addition, the thicknesses of the four layers of S-Polys were measured 2.84 nm at pH 6.5 and 2.95 nm at pH 3.5. The average thickness obtained from the TEM images is

shown in Figure 2C. The film

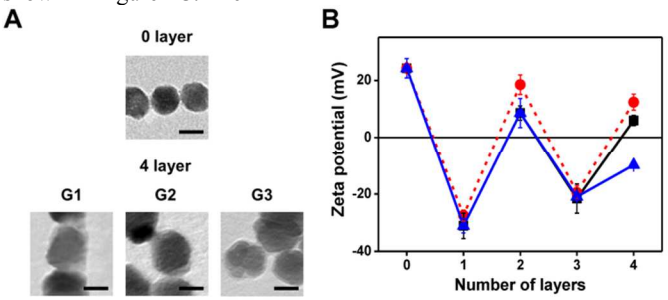


**Figure 3.** (A) EF-TEM micrographs of the MNPs and bFGF-loaded F-MNPs. The upper image shows the bare MNPs (0 layers), the bottom images show four layers of the bFGF-loaded F-MNPs: G1, G2, and G3, respectively. The scale bar is 20 nm. (B) Zeta-potential measurements of the bFGF-loaded F-MNPs for each layer. The original full-names of each of the bFGF-loaded F-MNPs are as follows: G1, $(HS/bFGF)_2$; G2, (HS/PLL/HS/bFGF); and G3, $(HS/bFGF/GO^-/PLL)$.

thicknesses increased linearly from 2.21 ± 0.46 nm to 3.39 ± 0.72 nm at pH 3.5 and from 1.82 ± 0.25 nm to 3.04 ± 0.45 nm at pH 6.5.

We also prepared Carbon F-MNPs. The GO lattice size is dramatically reduced upon ultrasonication[62]. During LbL deposition, each carbon layer was sunken down to reduce the overall size, and underwent sonication, resulting in the formation of nanoscale GO films (Figure S3†). For this reason, the films were finely deposited onto the MNPs. Thicknesses of the two and four layers were 4.7 nm and 8.1 nm, respectively (Figure 2A, bottom row). In general, the film morphologies vary slightly, depending on the materials used. For the S-Polys, the film structures showed dense packing at both the pH conditions, as compared to the carbon F-MNPs, which possessed rougher structures. We also measured the thicknesses of S-Poly and Carbon films on the silicon wafer for comparing with F-MNPs. As shown in Figure S2†, the thicknesses are increased linearly depending on number of bilayers. For S-Poly F-MNPs, the thicknesses were similar or less than S-Poly films on wafer (2 bilayers thicknesses of S-Poly films on wafer were 2.68 nm at pH 6.5 and 5.43 nm at pH 3.5 deducted from Figure S2A†). We consider that the different surface charge of MNPs and silicon result in smaller amount of polymers deposited on F-MNPs[63]. 1.5 times thicker films were deposited in case of Carbon F-MNPs than Carbon films on the silicon wafer (2 bilayers thickness of Carbon film on wafer was 5.38 nm). We suggest that the additionally bound GO sheets were not completely removed during washing step due to π–π interaction. Also after centrifuging at up to 12,000 rpm, F-MNPs remained surrounded with relatively large amounts of GO at the undermost of aliquot. The N-Poly based 2 and 4 layers of nanofilms (i.e., F-MNPs) are also confirmed by TEM (figure 2A). The N-poly film thickness is increased as a function of number of bilayers. The thickness of 4 layers is measured 1.84 nm which is similar to PLL/HA film prepared onto flat substrate (2 bilayers thickness is around 2.05 nm deducted from supplementary information: figure S2B†). Due to the pKa values of PLL and HA are around 9.36 and 3.08 respectively, the each material has relatively linear form at pH 6.0 due to their high intermolecular electrostatic repulsion. This phenomenon results the thickness of N-poly film measured relatively thin and have low roughness[46]. However, the PLL/HA film has highly interdiffused during film deposition, the film growth curve was displayed exponential growth behavior (figure S2B†)[46]. In Figure 2B, the ζ-potential results are shown as a function of the number of F-MNPs layers. All the F-MNPs (S-Poly, Carbon, and N-Poly) comprise surfaces with alternating charges, thereby ensuring the successful deposition of each layer of material onto the previous layer.

***Analysis of the bFGF-loaded F-MNPs***

During this study, the MNPs were further explored to see whether they could be used as efficient protein carriers by taking advantage of their magnetic properties[2,33]. Owing to their superparamagnetic properties, MNPs have been explored extensively in order to create new diagnostic procedures and drug delivery systems[5,8,64]. Some of the recent studies exploited the enhanced superparamagnetic properties of MNPs to demonstrate that they possess a much better nanocarrier efficacy when introduced into the target sites with the help of a magnetic field[2,33]. Figure 3A shows TEM images of the bFGF-loaded F-MNPs. Each F-MNP shows a unique composition. As shown in Figure 3A, the four layers of the G1 and G2 films barely seem to be present. However, for G3, the film was elaborately prepared with a thickness of approximately 2.81 nm. To determine the growth pattern of each film on the flat substrate, we also deposited the G1, G2, and G3 films onto a quartz glass substrate. The growth pattern was monitored by UV-Vis absorption spectra for every tetralayer (for G1, two bilayers). The absorbance band of HS is approximately 195 nm and the absorbance of HS increases linearly over every film (Figure S4†)[65]. However, the growth patterns are significantly different for the G1 and G2 films, and display less steep slopes than those for the G3 films. Moreover, the absorbance value at 195 nm is significantly higher than that for the G1 and G2 films, respectively. As shown in Figure S4†, for G1 and G2, the absorbance of the three tetralayers (six bilayers for G1) was approximately 0.01 nm, and for G3, it was approximately 0.15 nm. This absorbance value qualitatively implies that the thickness of the films and the density of the relevant vibration groups follows the Beer–Lambert Law[66]. For this reason, the TEM images of G1 and G2 are hardly distinguishable owing to a low absorbance value, whereas for the G3 film, they are clearly visible. These thickness values vary according to the pH condition for each film. The F-MNPs and the films on the quartz glass were fabricated in PBS (pH 7.4) and SAB buffers (pH 5.2), respectively, whereas the GO solution used a different condition (see the Materials and Methods section). The pI of bFGF is 9.6 and the pKa value of HS is approximately 3.0. In case of the HS/bFGF film, the HS is highly charged in a solution with a pH range of 5.2–7.4. Therefore, the deposited films showed a decreased thickness in this case. The G2 films also showed a similar result as the pKa of PLL is approximately 9.36[45]. However, GO was dissolved in DI water at a pH of 3.5. In the case of the G3 film, the deposited GO layer was thicker than the other layers as the pH was close to the pKa value (pKa = 4.3)[67]. We also measured the surface charge of the F-MNPs by using zeta-potential analysis at an interval of 1 layer (Figure 3B). The surface charge continuously changed for all of the FMNPs described above. The zeta-potential results clearly indicated that the films were deposited successfully onto the MNPs.

***Release mechanisms for the bFGF-loaded F-MNPs.***

In order to use F-MNPs for protein delivery, we precisely controlled the release kinetics by using physiologically relevant conditions by assembling the different material combinations of F-MNPs as described above (G1, G2, and G3, respectively). Figure 4A shows the normalized release of bFGF onto the various F-MNPs. Figure 4A (top image) simply depicts the experiment condition. We measured the bFGF release in α-MEM and each of the F-MNPs was dialyzed using a dialysis membrane to avoid the loss of F-MNPs during profiling. The molecular weight cut off (MWCO) of the dialysis membrane is 50 kDa; the bFGF (18 kDa) was thus

spontaneously released out of the membrane. We also studied and confirmed the effect of magnetic fields on bFGF release. Long and thin magnets was introduced into the dialysis membrane during the

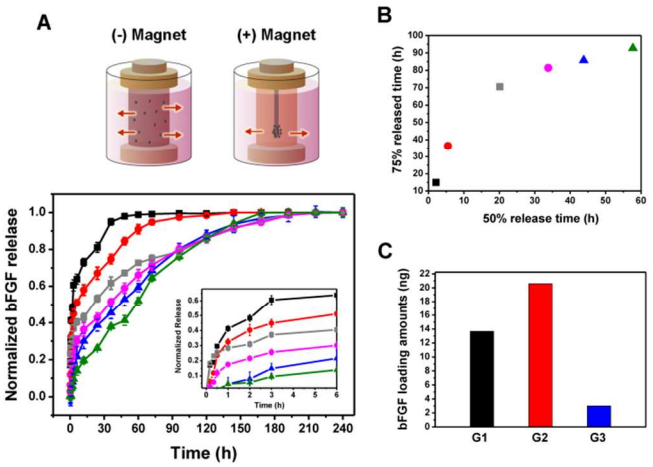


**Figure 4.** (A) Top: Simple illustration for assessing the modes of bFGF release for the various bFGF-loaded F-MNPs. Bottom: Normalized bFGF-released profiles of the bFGF-loaded F-MNPs: (-) magnet G1, (■, black line); (-) magnet G2, (●, red line); (-) magnet G3, (▲, blue line); (+) magnet G1, (■, gray line); (+) magnet G2, (●, pink line); and (+) magnet G3, (▲, green line). (B) Various bFGF release times for the F-MNPs. (C) The bFGF loading amounts for 50 mg of F-MNPs

measurement. We named magnetic treated group "(+) magnet". In other way, an untreated group was named by "(-) magnet". And all groups were depicted simplify in figure 4A top. While mixing F-MNPs with α-MEM, the suspension turned from bright pink to dark brown because of the dispersion of F-MNPs ((-) magnet). As in the figure, for (+) magnet, the magnet was inside the membrane and F-MNPs were stuck to the magnet strongly. Therefore, when the magnet was introduced into the suspension, the suspension was immediately restored to the previous color and the F-MNPs stuck to the magnets. The collected F-MNPs ((+) magnet) showed a decreased superficial contact with α-MEM in the absence of a magnet ((-) magnet), and resulted into a sustained release, as described in Figure 4A (at the bottom of the panel). The graph indicates that each of the F-MNPs showed a unique manner of release, depending on their unique film compositions. For the F-MNPs in the absence of any magnets, the burst release result was obtained for the G1 and G2 films, and the $t_{1/2}$ for the release time was over 2.14 h and 5.5 h, respectively (Figure 4B). Typically, bFGF is a small globular protein possessing a low charge density. Therefore, when the films incorporating bFGF were exposed to the MEM conditions, bFGF rapidly lost its charge owing to the high-salt condition (as compared to those during the deposition process), and easily diffused out of the films[68]. Therefore, the G1 film that only deposited with HS and bFGF showed a diminished interdiffusion and stability, and thus was easy to erode under physiological conditions. On the contrary, for the polypeptide PLL-incorporated film (G2), the molecular weight was more than 10 times higher than that for HS and bFGF, owing to which it incorporated and trapped bFGF into the film layer[69]. As shown in Figures 4B and 4C, the G2 film showed a sustained release and incorporated about 1.5 times more bFGF than the G1 film did.

bFGF was released slower in the G3 film, than in the G1 and G2 films, and a 50% and 75% release time was gained after 43.83 h and 85.79 h, respectively (Figures 4A and 4B). Unlike the G1 and G2 films, the G3 film showed an extremely sustained release. This result was attributed to the low permeability of GO. bFGF, which was previous deposited under GO, was blocked out from the GO layer, resulting into a sustained release[43]. The 50% and 75% release times

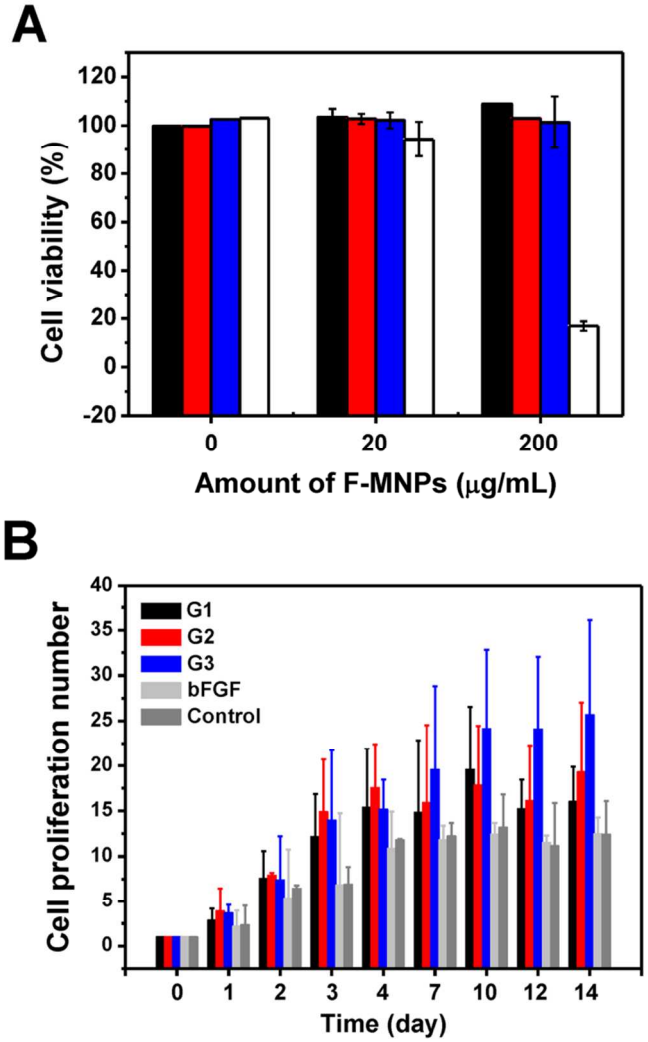


**Figure 5.** (A) The hDF viability of the MNPs and bFGF-loaded F-MNPs; black: G1, red: G2, blue: G3, and white: MNPs. (B) Proliferative effects of bFGF-loaded F-MNPs on hDF: bare bFGF treated group (right gray), G1 (black), G2 (red), G3 (blue) and control group (gray). The control is untreated with bFGF during 14 days (negative control)

for each of the F-MNPs are depicted in Figure 4B. In conclusion, we could prepare various F-MNPs exhibiting diverse loading capacities and release profiles by simply changing the film combinations.

***In vitro experiments on bFGF-loaded F-MNPs***

To test whether the bFGF-loaded F-MNPs were suitable for biomedical applications, we also carried out the cell viability test for hDFs. Figure 5A shows the hDF viability test results for the MNPs and the G films. At a low concentration (20 μg/mL), none of the MNPs and G films exhibited cytotoxicity on the hDFs (>100%). However, most of cells (≈ 83%) died at higher concentrations, indicating that the MNPs negatively affect the cells. The G films showed high cell viability despite being treated with high concentrations (200 μg/mL). In the case of MNPs, the particles aggregated easily and induced cell death during the treatment

(Figure S5†). However, the G films show a less (or completely absent) aggregation effect and result in higher cell viability. Therefore, we conclude that the biocompatible materials coated with MNPs show no cytotoxic effects on hDF.

In order to investigate the protein loading and delivery capacity of bFGF-loaded F-MNPs, we also conducted a cell proliferation test. Figure 5B is the normalized proliferation increase of hDF number during the 14 days after treatment. For treating the same amount of bFGF on hDF, we treated different volumes of each F-MNPs by ratio of bFGF loading amount (Figure 4C). As indicated in Figure 5B, F-MNPs treated cells were more proliferated than bare bFGF treated cells over 14 days.

Heparin is known as a material that maintains bFGF activity[70]. In the case of only the bFGF treated group, therefore, the bFGF lost their stability and activity and hDF proliferated as same as control group (bFGF untreated cells). The bFGF released from the F-MNPs was stable and acted on hDF after the 14 day treatment. For that reason, the incorporated bFGF with heparin onto MNPs conserves bFGF over 14 days. Also each F-MNP (G1, G2 and G3) had a different cell proliferation property, for G2 and G3 had cell proliferation property than G1 throughout 14 days. The interdiffused and blocked bFGF (G2 and G3) was slowly released out of the films and, as a result, acted on hDF over a long period of time. In particular, G3 exhibited the highest proliferation among the F-MNPs, as GO is known to promote cell proliferation, and thus the incorporated GO layer induced hDF proliferation with bFGF blocking function[71,72].

## Conclusions

In this study, we focused on the characterization of MNPs and F-MNPs. The synthesized MNPs possess a diameter of approximately 30 nm and show a narrow size distribution, well stabilized by dodecylamine, as evident from the TEM and zeta-potential results, respectively. We successfully deposited films with PAA/PAH, $GO^-/GO^+$, and HA/PLL combinations onto the MNPs. For the weak polyelectrolytes, the films showed different thicknesses and morphologies depending on the pH value. Furthermore, for protein delivery, three types of bFGF-loaded F-MNPs comprising different building materials and compositions showed unique release profiles and loading properties. The bFGF-loaded F-MNPs were not toxic to hDFs and helped hDFs proliferate more than pure bFGF. By taking complete advantage of the LbL assembly, we could fabricate F-MNPs with various materials, from carbon materials to growth factors. We also showed that MNPs could be used in biomedical applications. In summary, the LbL assembly method and the functionalized nanoparticles could be used for various biomedical applications.

## Acknowledgements

This research was supported by the National Research Foundation of Korea (NRF), funded by the Ministry of Science, ICT & Future Planning NRF-2013R1A1A1076126, and 2014060751. Additionally, this work was also supported by a grant from the Next-Generation BioGreen 21 Program (No. PJ009986012014) (Rural Development Administration, Republic of Korea), as well as the High Value-added Food Technology Development Program of the Ministry of Agriculture, Food and Rural Affairs (114027-03-1-HD020).

**Notes and referencess**

[a] School of Chemical Engineering & Material Science, Chung-Ang University, 47 Heukseok-ro, Dongjak-gu, Seoul 156-756, Republic of Korea
[b] School of Chemical and Biological Engineering, Seoul National University, 1 Gwanak-ro, Gwanak-gu, Seoul 151-742, Republic of Korea
[c] Advanced Institutes of Convergence Technology, 145 Gwanggyo-ro, Yeongtong-gu, Suwon 443-270, Republic of Korea

† Footnotes should appear here. These might include comments relevant to but not central to the matter under discussion, limited experimental and spectral data, and crystallographic data.

Electronic Supplementary Information (ESI) available: [details of any supplementary information available should be included here]. See DOI: 10.1039/b000000x/

1. M.-R. Choi, K. J. Stanton-Maxey, J. K. Stanley, C. S. Levin, R. Bardhan, D. Akin, S. Badve, J. Sturgis, J. P. Robinson and R. Bashir, Nano letters, 2007, 7, 3759-3765.
2. M. Arsianti, M. Lim, C. P. Marquis and R. Amal, Langmuir : the ACS journal of surfaces and colloids, 2010, 26, 7314-7326.
3. T. Imoto, T. Kida, M. Matsusaki and M. Akashi, Macromolecular bioscience, 2010, 10, 271-277.
4. Z. Li, J. C. Barnes, A. Bosoy, J. F. Stoddart and J. I. Zink, Chemical Society reviews, 2012, 41, 2590-2605.
5. S. Gelperina, K. Kisich, M. D. Iseman and L. Heifets, American journal of respiratory and critical care medicine, 2005, 172, 1487-1490.
6. A. K. Gupta and M. Gupta, Biomaterials, 2005, 26, 3995-4021.
7. L. Zhang, F. Gu, J. Chan, A. Wang, R. Langer and O. Farokhzad, Clinical Pharmacology & Therapeutics, 2007, 83, 761-769.
8. R. Hao, R. Xing, Z. Xu, Y. Hou, S. Gao and S. Sun, Advanced materials, 2010, 22, 2729-2742.
9. P. Majewski and B. Thierry, Critical Reviews in Solid State and Materials Sciences, 2007, 32, 203-215.
10. J. Cheon and J.-H. Lee, Accounts of chemical research, 2008, 41, 1630-1640.
11. T. Neuberger, B. Schöpf, H. Hofmann, M. Hofmann and B. Von Rechenberg, Journal of Magnetism and Magnetic Materials, 2005, 293, 483-496.
12. M. Lewin, N. Carlesso, C.-H. Tung, X.-W. Tang, D. Cory, D. T. Scadden and R. Weissleder, Nature biotechnology, 2000, 18, 410-414.
13. J. Gao, L. Li, P. L. Ho, G. C. Mak, H. Gu and B. Xu, Advanced materials, 2006, 18, 3145-3148.
14. C. S. Love, I. Ashworth, C. Brennan, V. Chechik and D. K. Smith, Langmuir : the ACS journal of surfaces and colloids, 2007, 23, 5787-5794.
15. L. Pan, Q. He, J. Liu, Y. Chen, M. Ma, L. Zhang and J. Shi, Journal of the American Chemical Society, 2012, 134, 5722-5725.
16. R. Guillet-Nicolas, A. Popat, J. L. Bridot, G. Monteith, S. Z. Qiao and F. Kleitz, Angewandte Chemie, 2013, 125, 2374-2378.
17. A. L. Martin, L. M. Bernas, B. K. Rutt, P. J. Foster and E. R. Gillies, Bioconjugate chemistry, 2008, 19, 2375-2384.
18. R. Mout, D. F. Moyano, S. Rana and V. M. Rotello, Chem. Soc. Rev., 2012, 41, 2539-2544.
19. Y. Liu, D. Tu, H. Zhu and X. Chen, Chemical Society reviews, 2013, 42, 6924-6958.
20. J. Kost and R. Langer, Advanced drug delivery reviews, 2012, 64,

327-341.
21. G. Decher, Science, 1997, 277, 1232-1237.
22. F. Caruso, R. A. Caruso and H. Möhwald, Science, 1998, 282, 1111-1114.
23. J. B. Schlenoff, S. T. Dubas and T. Farhat, Langmuir : the ACS journal of surfaces and colloids, 2000, 16, 9968-9969.
24. J. Cho, K. Char, J. D. Hong and K. B. Lee, Advanced materials, 2001, 13, 1076-1078.
25. K. C. Wood, J. Q. Boedicker, D. M. Lynn and P. T. Hammond, Langmuir : the ACS journal of surfaces and colloids, 2005, 21, 1603-1609.
26. X. Su, B.-S. Kim, S. R. Kim, P. T. Hammond and D. J. Irvine, Acs Nano, 2009, 3, 3719-3729.
27. J. Hong, B.-S. Kim, K. Char and P. T. Hammond, Biomacromolecules, 2011, 12, 2975-2981.
28. M. Matsusaki, H. Ajiro, T. Kida, T. Serizawa and M. Akashi, Advanced materials, 2012, 24, 454-474.
29. K. Ariga, Y. Lvov and T. Kunitake, Journal of the American Chemical Society, 1997, 119, 2224-2231.
30. K. Kadowaki, M. Matsusaki and M. Akashi, Langmuir : the ACS journal of surfaces and colloids, 2010, 26, 5670-5678.
31. P. T. Hammond, AIChE Journal, 2011, 57, 2928-2940.
32. D. I. Gittins and F. Caruso, Advanced materials, 2000, 12, 1947-1949.
33. B. Thierry, F. Al-Ejeh, A. Khatri, Z. Yuan, P. J. Russell, S. Ping, M. P. Brown and P. Majewski, Chem. Commun., 2009, 7348-7350.
34. Z. Poon, J. B. Lee, S. W. Morton and P. T. Hammond, Nano letters, 2011, 11, 2096-2103.
35. G. F. Schneider, V. Subr, K. Ulbrich and G. Decher, Nano letters, 2009, 9, 636-642.
36. S. W. Morton, Z. Poon and P. T. Hammond, Biomaterials, 2013, 34, 5328-5335.
37. Y. Yan, M. Björnmalm and F. Caruso, Chemistry of Materials, 2013, 26, 452-460.
38. E. C. Dreaden, S. W. Morton, K. E. Shopsowitz, J. H. Choi, Z. J. Deng, N.-J. Cho and P. T. Hammond, ACS nano, 2014, 8, 8374-8382.
39. F. Caruso, H. Lichtenfeld, M. Giersig and H. Möhwald, Journal of the American Chemical Society, 1998, 120, 8523-8524.
40. J. Hong, W. K. Bae, H. Lee, S. Oh, K. Char, F. Caruso and J. Cho, Advanced materials, 2007, 19, 4364-4369.
41. S. S. Shiratori and M. F. Rubner, Macromolecules, 2000, 33, 4213-4219.
42. J. Hong, J. Y. Han, H. Yoon, P. Joo, T. Lee, E. Seo, K. Char and B.-S. Kim, Nanoscale, 2011, 3, 4515-4531.
43. J. Hong, N. J. Shah, A. C. Drake, P. C. DeMuth, J. B. Lee, J. Chen and P. T. Hammond, Acs Nano, 2011, 6, 81-88.
44. S. Asayama, M. Nogawa, Y. Takei, T. Akaike and A. Maruyama, Bioconjugate chemistry, 1998, 9, 476-481.
45. S. E. Burke and C. J. Barrett, Biomacromolecules, 2003, 4, 1773-1783.
46. Y. Lee, H. Lee, Y. B. Kim, J. Kim, T. Hyeon, H. Park, P. B. Messersmith and T. G. Park, Advanced materials, 2008, 20, 4154-4157.
47. L. Schweigerer, G. Neufeld, J. Friedman, J. A. Abraham, J. C. Fiddes and D. Gospodarowicz, Nature, 1987, 325, 257-259.
48. M. Klagsbrun, Progress in growth factor research, 1989, 1, 207-235.
49. M. L. Macdonald, N. M. Rodriguez, N. J. Shah and P. T. Hammond, Biomacromolecules, 2010, 11, 2053-2059.
50. D. G. Greenhalgh, K. Sprugel, M. Murray and R. Ross, The American journal of pathology, 1990, 136, 1235.
51. S. Yoshimura, Y. Takagi, J. Harada, T. Teramoto, S. S. Thomas, C. Waeber, J. C. Bakowska, X. O. Breakefield and M. A. Moskowitz, Proceedings of the National Academy of Sciences, 2001, 98, 5874-5879.
52. J. De Haro, F. Acin, A. Lopez-Quintana, A. Florez, E. Martinez-Aguilar and C. Varela, Heart and vessels, 2009, 24, 321-328.
53. T. Hashimoto, H. Koyama, T. Miyata, A. Hosaka, Y. Tabata, T. Takato and H. Nagawa, European Journal of Vascular and Endovascular Surgery, 2009, 38, 71-75.
54. M. Klagsbrun, Current opinion in cell biology, 1990, 2, 857-863.
55. S. Faham, R. Hileman, J. Fromm, R. Linhardt and D. Rees, Science, 1996, 271, 1116-1120.
56. K. Masuoka, M. Ishihara, T. Asazuma, H. Hattori, T. Matsui, B. Takase, Y. Kanatani, M. Fujita, Y. Saito and H. Yura, Biomaterials, 2005, 26, 3277-3284.
57. N. I. Kovtyukhova, P. J. Ollivier, B. R. Martin, T. E. Mallouk, S. A. Chizhik, E. V. Buzaneva and A. D. Gorchinskiy, Chemistry of Materials, 1999, 11, 771-778.
58. M. Aslam, E. A. Schultz, T. Sun, T. Meade and V. P. Dravid, Crystal growth & design, 2007, 7, 471-475.
59. Y. Yu, M. Zhou, W. Shen, H. Zhang, Q. Cao and H. Cui, Carbon, 2012, 50, 2539-2545.
60. D. Yoo, S. S. Shiratori and M. F. Rubner, Macromolecules, 1998, 31, 4309-4318.
61. J. Choi and M. F. Rubner, Macromolecules, 2005, 38, 116-124.
62. A. Ciesielski and P. Samorì, Chemical Society reviews, 2014, 43, 381-398.
63. V. Kozlovskaya, S. Ok, A. Sousa, M. Libera and S. A. Sukhishvili, Macromolecules, 2003, 36, 8590-8592.
64. C. C. Berry and A. S. Curtis, Journal of physics D: Applied physics, 2003, 36, R198.
65. Y. Shu, P. Yin, B. Liang, S. Wang, L. Gao, H. Wang and L. Guo, Journal of Materials Chemistry, 2012, 22, 21667-21672.
66. D. Li and J. Brisson, Polymer, 1998, 39, 793-800.
67. B. Konkena and S. Vasudevan, The Journal of Physical Chemistry Letters, 2012, 3, 867-872.
68. C. Picart, Current medicinal chemistry, 2008, 15, 685-697.
69. A. Shukla, S. N. Avadhany, J. C. Fang and P. T. Hammond, Small, 2010, 6, 2392-2404.
70. G. Chen, D. R. Gulbranson, P. Yu, Z. Hou and J. A. Thomson, Stem Cells, 2012, 30, 623-630.
71. M. Kalbacova, A. Broz, J. Kong and M. Kalbac, Carbon, 2010, 48, 4323-4329.
72. W. C. Lee, C. H. Y. Lim, H. Shi, L. A. Tang, Y. Wang, C. T. Lim and K. P. Loh, ACS nano, 2011, 5, 7334-7341.



 